Available online at www.sciencedirect.com
SCIENCE DIRECT®
Polymer 44 (2003) 6815–6823
polymer
www.elsevier.com/locate/polymer

Phase behavior of linear polystyrene-*block*-poly(2-vinylpyridine)-*block*-poly(*tert*-butyl methacrylate) triblock terpolymers

Sabine Ludwigs[a], Alexander Böker[a,b], Volker Abetz[b,*], Axel H.E. Müller[b,c], Georg Krausch[a,c,*]

[a]*Physikalische Chemie II, Universität Bayreuth, D-95440 Bayreuth, Germany*
[b]*Makromolekulare Chemie II, Universität Bayreuth, D-95440 Bayreuth, Germany*
[c]*Bayreuther Zentrum für Kolloide und Grenzflächen (BZKG), Universität Bayreuth, D-95440 Bayreuth, Germany*

Received 11 March 2003; received in revised form 11 July 2003; accepted 23 July 2003

Abstract

Using sequential living anionic polymerization we synthesized well-defined linear ABC triblock terpolymers from polystyrene (PS), poly(2-vinylpyridine) (P2VP), and poly(*tert*-butyl methacrylate) (PtBMA). The length of the PtBMA block was systematically increased at constant block length ratios of the PS and P2VP blocks. The microdomain structures were characterized by transmission electron microscopy (TEM) and small angle X-ray scattering (SAXS). With increasing PtBMA block size we observe a systematic change in the bulk structure of the block copolymers.

Keywords: Anionic polymerization; Triblock terpolymers; Small angle X-ray scattering

1. Introduction

In recent years ternary triblock terpolymers have attracted increasing interest owing to their rich variety of bulk morphologies [1–3]. The latter is due to the large number of independent molecular parameters characterizing these materials. In addition to the degree of polymerization and the different mutual segmental interactions also the composition and the chain topology control the phase behavior in the melt. Ternary triblock terpolymers may form core-shell analogs of the well-known diblock copolymer morphologies, where the middle block forms a layer between the two outer blocks [3–5]. Alternatively, the middle block may form spheres or cylinders between the two outer blocks [1,6]. In addition, structures with the middle block forming the matrix around cylinders or spheres of the outer blocks [4] or systems where only one outer block forms dispersed domains in a lamella of the middle block are known [7]. Among the most fascinating morphologies is a helical morphology, in which one end block forms a cylinder, which is helically surrounded by cylindrical midblock domains, both embedded in a matrix of the other end block [6]. Finally, a core-shell double gyroid structure has been observed, in which one end block forms the two gyroids, which are surrounded by shells of the midblock and the other outer block fills the space between these two core-shell gyroids [3,5,8,9].

We have recently reported on first experiments investigating the thin film behavior of ABC triblock terpolymers [10–14]. In the presence of boundary surfaces and confined to a thickness comparable to the characteristic bulk spacing, the microdomain structures of block copolymers can significantly differ from the respective bulk structures. Both large-scale alignment of the microdomains as well as the formation of novel microdomain structures has been observed [15,16]. For the particular case of a polystyrene-*block*-poly(2-vinylpyridine)-*block*-poly(*tert*-butyl methacrylate) (SVT) triblock terpolymer with volume fractions $\phi_S : \phi_V : \phi_T$ scaling as 1:1.4:3 a particularly rich variety of thin film structures was found. In order to be able to study these phenomena more systematically, we have synthesized two series of triblock terpolymers, which exhibit a certain constant ratio between the PS and P2VP blocks, while the volume fraction of the PtBMA block was stepwise increased within each series. The goal of this procedure is to systematically explore certain regions of the ternary phase diagram. Here, we summarize our synthetic results and

* Corresponding authors. Tel.: +49-921-553395; fax: +49-921-553393.
E-mail addresses: volker.abetz@uni-bayreuth.de (V. Abetz), georg.krausch@uni-bayreuth.de (G. Krausch).

0032-3861/$ - see front matter © 2003 Elsevier Ltd. All rights reserved.
doi:10.1016/j.polymer.2003.07.001

describe the bulk structures found for the various materials as a function of composition. While a systematic variation of the length of the middle block requires the complete synthesis procedure for each triblock terpolymer [1,4], in the case of the variation of the last triblock a sequential addition of the last monomer can lead to a series of triblock terpolymers having exactly the same diblock copolymer precursor [17].

Our approach is based on earlier work by Giebeler et al. who first synthesized SVT triblock terpolymers [18] aiming at the investigation of their amphiphilic behavior after the hydrolysis of the PtBMA block, which leads to a block polyelectrolyte.

2. Experimental section

2.1. Synthesis of SVT triblock terpolymers

The linear SVT triblock terpolymers were synthesized via sequential living anionic polymerization in THF using *sec*-butyl lithium as initiator [18]. Both after polymerization of the PS block and of the P2VP block, 1,1-diphenylethylene was added to end-cap the living ends of the anions. In this way crossover steps and transfer reactions due to too high nucleophilicity could be suppressed. During the polymerization of the PtBMA block, samples were taken from the reactor after different polymerization times and were precipitated into degassed methanol. Thus we could obtain a series of polymers with constant ratio of the PS and P2VP blocks, but with increasing length of the PtBMA end block.

We synthesized two series with the above-described procedure, one series with volume fractions $\phi_S : \phi_V : \phi_T = 1 : 1.2 : x$ (x increasing) and the other with $\phi_S : \phi_V : \phi_T = 1 : 1.4 : x$ (x increasing). Gel permeation chromatography (GPC) measurements were performed on a set of 30 cm SDV-gel columns of 5 μm particle size having a pore size of 10^5, 10^4, 10^3 and 10^2 Å with refractive index and UV ($\lambda = 254$ nm) detection. GPC was measured at an elution rate of 1 ml/min with THF as solvent. The calibration was based on narrowly distributed polystyrene standards. Fig. 1 shows the GPC trace (RI signal) of the triblock terpolymer with the highest amount of PtBMA and its precursors PS and PS-*b*-P2VP. The number-averaged molecular weight of the polystyrene precursor and the molecular weight distributions of the triblock terpolymers were determined by this method. All polymers exhibit a narrow molecular weight distribution characterized by a polydispersity between 1.01 and 1.05. A quantitative evaluation of the respective peaks in the GPC trace shows that the relative amount of diblock copolymer and homopolymer is less than 1%. The polydispersity index does not include the contributions of homopolymer and diblock precursor, however, an estimate shows that due to the small amounts the actual numbers would not significantly change if the precursors would be included. Additionally, ^{1}H NMR

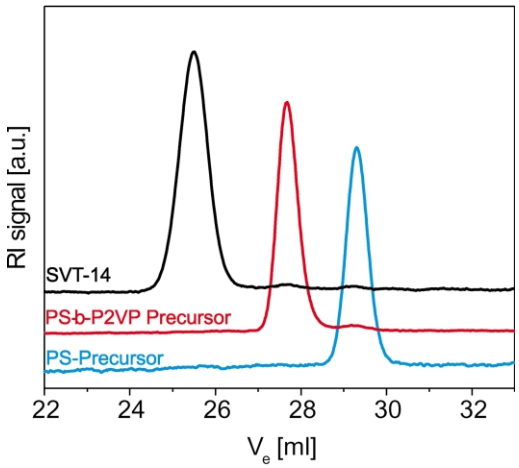

Fig. 1. GPC trace (RI signal) of triblock terpolymer $S_{16}V_{21}T_{63}^{140}$ and its precursors PS and PS-*b*-P2VP. $M_w = 140{,}000$ g/mol; $M_w/M_n = 1.03$.

spectra were acquired on a 250 MHz Bruker AC spectrometer using $CDCl_3$ as solvent and tetramethylsilane (TMS) as internal standard. The molecular weights of the P2VP and the PtBMA blocks were calculated using the triblock terpolymer composition determined by NMR and the polystyrene molecular weights from GPC. Table 1 summarizes the molecular parameters of the resulting materials.

2.2. Structural characterization

For structural characterization films of the SVT triblock terpolymers were cast from $CHCl_3$ solution by slowly evaporating the solvent for several days. The films were

Table 1
Block copolymer molecular characteristics

Polymer[a]	M_w (kg/mol)	M_w/M_n	$\phi_{PS} : \phi_{P2VP} : \phi_{PtBMA}$	Bulk morphology[b]
$S_{16}V_{21}T_{63}^{140}$	140	1.03	1:1.2:4	CYL
$S_{17}V_{22}T_{61}^{132}$	132	1.03	1:1.2:3.65	GYR, PL
$S_{17}V_{23}T_{60}^{129}$	129	1.03	1:1.2:3.39	GYR, PL
$S_{18}V_{24}T_{58}^{124}$	124	1.03	1:1.2:3.33	GYR, PL
$S_{19}V_{25}T_{56}^{120}$	120	1.03	1:1.2:3.05	GYR, PL
$S_{25}V_{33}T_{42}^{90}$	90	1.04	1:1.2:1.76	L
$S_{27}V_{35}T_{38}^{84}$	84	1.04	1:1.2:1.39	L
$S_{30}V_{39}T_{31}^{77}$	77	1.04	1:1.2:1.13	L
$S_{30}V_{40}T_{30}^{74}$	74	1.04	1:1.2:1	GYR
$S_{32}V_{42}T_{26}^{70}$	70	1.05	1:1.2:0.82	GYR
$S_{34}V_{45}T_{21}^{66}$	66	1.05	1:1.2:0.66	GYR
$S_{35}V_{52}T_{13}^{82}$	82	1.02	1:1.4:0.39	GYR
$S_{36}V_{54}T_{10}^{80}$	80	1.02	1:1.4:0.30	UL
$S_{37}V_{55}T_{8}^{78}$	78	1.01	1:1.4:0.24	UL
$S_{38}V_{56}T_{6}^{76}$	76	1.01	1:1.4:0.15	GYR
$S_{43}V_{57}^{52}$	52	1.01	1:1.2	L
$S_{40}V_{60}^{72}$	72	1.01	1:1.4	L

[a] $S_{\%S}V_{\%V}T_{\%T}^{M_w}$ with the subsripts representing the weight fractions of the respective blocks (parts in hundred), while M_w is the overall weight-averaged molecular weight in kg/mol.

[b] Key: CYL, core-shell-cylinder; GYR, core-shell-gyroid; PL, perforated lamellae; L, lamellae; UL, undulated lamellae.

subsequently dried under vacuum for 4 days at 50 °C. Extended annealing (several days) at temperatures well above the glass transition temperatures of the three block components did not lead to any changes in the microdomain structure. In addition to the melt samples, we have investigated the microdomain structure prior to drying in chloroform solutions with different concentrations.

For transmission electron microscopy (TEM) 30–60 nm thick sections were cut from the as-cast films. All TEM micrographs were taken on a Zeiss transmission electron microscope (CEM 902) operating at 80 kV in the bright field mode. In order to enhance the electron density contrast between the three phases the samples were stained with RuO_4 and I_2, respectively. On staining with RuO_4 the PS and P2VP phases are expected to appear dark and grey, respectively, in the TEM images, while the PtBMA phase should remain unstained and appear bright. Exposure of the samples to I_2 on the other hand leads to a preferential staining of the P2VP phase. One should keep in mind, though, that staining often is not selective enough to establish an unambiguous contrast between all three polymer components. Furthermore, it is well-known that electron beam damage can lead to considerable volume shrinkage of polymethacrylate phases [19].

Small angle X-ray scattering (SAXS) measurements were performed at the ID2 beamline at the European Synchrotron Radiation Facility (ESRF, Grenoble, France). The typical photon flux obtained at the ID2 sample position is 8×10^{12} photons/s, the energy bandwidth is $\Delta E/E = 2 \times 10^{-4}$. All experiments were obtained at 12.5 keV corresponding to an X-ray wavelength of 0.1 nm. The scattering intensities were detected via a CCD camera. The detector system is housed in a 10 m evacuated flight tube. The scattering patterns were corrected for the beam stop and the background prior to evaluations. The calculations of the scattering intensities were obtained with the Fit2D evaluation program [20].

To estimate the scattering contrast between the three components PS, P2VP and PtBMA, we have calculated their electron densities: $\rho_e(\mathrm{PS}) = 0.566$ mol/cm^3; $\rho_e(\mathrm{P2VP}) = 0.611$ mol/cm^3 and $\rho_e(\mathrm{PtBMA}) = 0.561$ mol/cm^3. As the values of PS and PtBMA are very similar, we expect only a weak scattering contrast between the two end blocks of the triblock terpolymers.

3. Results and discussion

In the following we summarize the results on the microdomain structure of the materials. Depending on the length of the PtBMA block we can identify six different regions of characteristic bulk structures in the phase diagram. We present the results obtained for six characteristic block copolymers—the remaining materials resemble one of the six and will only briefly be discussed below. We start with the largest PtBMA volume fractions and move towards decreasing PtBMA content. We use the notation of the block copolymers given in Table 1, i.e. we denote the polymers as $S_{\%S}V_{\%V}T^{M_w}_{\%T}$ with the subscripts representing the weight fractions of the respective blocks (parts in hundred), while M_w is the overall weight-averaged molecular weight in kg/mol.

3.1. $S_{16}V_{21}T^{140}_{63}$: core-shell cylinders

Fig. 2(a) shows a transmission electron micrograph of $S_{16}V_{21}T^{140}_{63}$ after staining with I_2. P2VP appears as dark phase. A slightly distorted hexagonal arrangement of dark cylinder heads can be recognized, which is in accordance

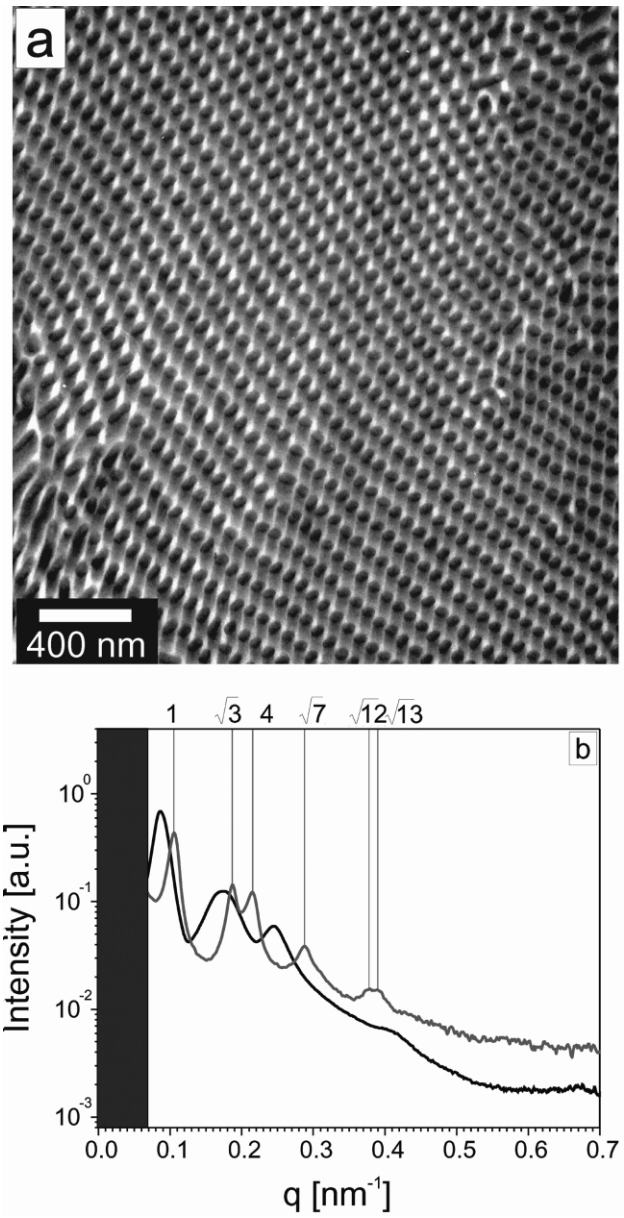

Fig. 2. $S_{16}V_{21}T^{140}_{63}$ (a) TEM micrograph, stained with I_2 (dark phase: P2VP); (b) SAXS pattern of a 36 wt% chloroform solution (grey curve) and the dry state (dark curve) ($q = 4\pi/\lambda \sin\theta$; λ = wavelength, 2θ = scattering angle), typical cylindrical reflex positions.

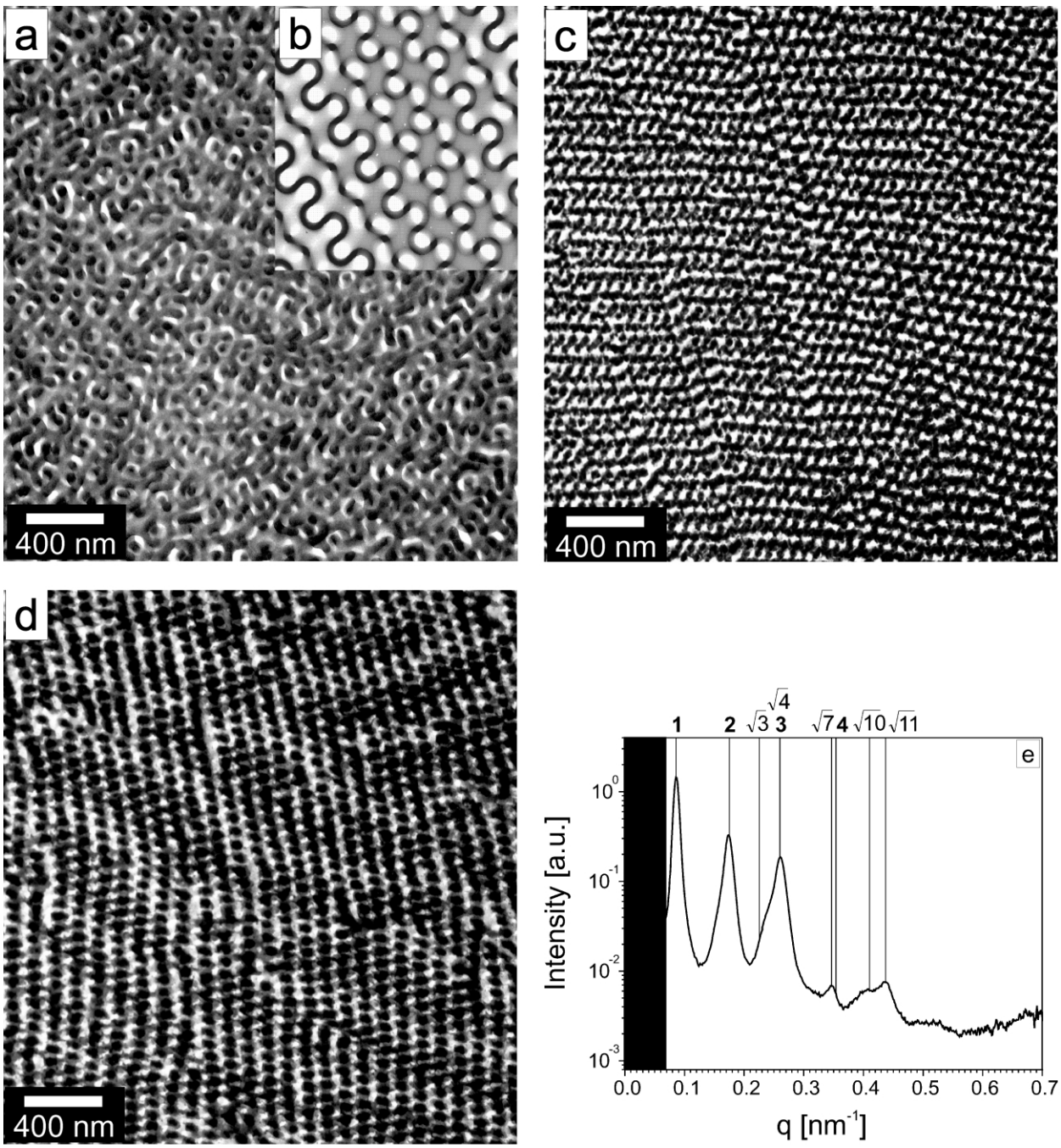

Fig. 3. $S_{19}V_{25}T_{56}^{120}$ (a), (c) and (d) TEM micrographs; (a) stained with I_2 (dark phase: P2VP); (c) and (d) stained with RuO_4 (bright phase: PtBMA, dark phase: PS/P2VP; (b) TEMsim simulation of the '[1.08;0.84;2.04]' projection (dark matrix, translation 0.48, thickness 0.35) [21,22]; (e) SAXS ($q = 4\pi/\lambda \sin\theta$; λ = wavelength, 2θ = scattering angle), reflex positions typical for a lamellar (bold-faced printed figures) and a gyroid structure (as [211] reflection).

with the SAXS data. Fig. 2(b) shows the SAXS data for a 36 wt% SVT solution in chloroform and for a solvent-annealed dry film (prepared in the manner described above). The scattering maxima appear at relative positions of $1{:}\sqrt{3}{:}2{:}\sqrt{7}{:}\sqrt{12}{:}\sqrt{13}$, which correspond to the [100], [110], [200], [210], [220] and [310] reflections of a hexagonal cylindrical structure. The [300] peak is not visible. The SAXS pattern of the solution clearly exhibits the peaks characteristic of a cylindrical structure, while on the dry sample the [110] and [200] reflections cannot be clearly distinguished because of peak broadening. This might be due to preparation effects. However, it can be clearly seen that the peaks shift to smaller q values, which is typical for our system as the spacing of the long period is growing with increasing polymer concentration with a maximum value for the bulk structure.

Considering the volume fractions of the blocks, we assume a core-shell-cylinder-morphology with PS-core

surrounded by a P2VP-shell embedded within a PtBMA matrix phase.

3.2. $S_{19}V_{25}T_{56}^{120}$: via core-shell gyroid towards lamellae

Upon reduction of the PtBMA volume fraction, the microdomain structure changes. Fig. 3(a), (c) and (d) show TEM micrographs taken at different spots of the sample. Three different structures can be identified: the structure shown in Fig. 3(a) can best be interpreted as a gyroid structure. For comparison, in Fig. 3(b) we show simulation results of the [1.08;0.84;2.04] projection of the cubic lattice of a double-gyroid structure [21,22]. Note that the presentation of the Miller indices in non-integer numbers is given to show that the observed projection is not exactly the [112] projection, but very close to that. In Fig. 3(c) three-fold projections (stripe-like pattern) are found while Fig. 3(d) shows four-fold projections (pearl-like structure). In Fig. 3(c) and (d) staining was achieved with RuO_4, while in Fig. 3(a) I_2 was used. In Fig. 3(e), the corresponding SAXS pattern is shown. The pattern is rather complex and may be interpreted as a superposition of scattering patterns resulting from at least two coexisting structures. The three maxima with relative positions of 1:2:3 are typical for a lamellar structure. Additionally, an assignment of the scattering maxima of a gyroid morphology can be discussed under the assumption that the shoulder at the $\sqrt{3}$-position is corresponding to the [211]-reflection. The relative ratios of the maxima of a gyroid morphology are: $\sqrt{3}$:$\sqrt{4}$: $\sqrt{7}$:$\sqrt{10}$:$\sqrt{11}$. The scattering patterns of gyroid morphologies have been discussed before [23,24].

We assume that parts of the material form a core-shell-gyroid with PS-cores surrounded by P2VP shells embedded within a PtBMA matrix. Fig. 3(c) and (d) show a preferential direction of the stripe-like and pearl-like structures. This could cause the lamellar arrangement of the scattering maxima in the SAXS profile. We anticipate the coexistence of perforated lamellae with PtBMA channels (matrix component) connecting between two sheets of PtBMA in a lamellar structure. Up to now the morphology of perforated lamellae has only been found in diblock copolymers [25,26], and in blends of ABC and AD block copolymers [27]. From self-consistent field theory it follows that perforated lamellae are not stable in the case of diblock copolymers [28]. Recently, this result has been verified experimentally for a number of diblock copolymers, including polystyrene-*b*-polyisoprene (PS-*b*-PI), polystyrene-*b*-poly(2-vinylpyridine) (PS-*b*-P2VP), and poly(ethylene oxide)-*b*-poly(ethyl ethylene) (PEO-*b*-PEE) [26, 29–33]. In these cases a transition from perforated lamellae to a bicontinuous gyroid structure was observed upon isothermal annealing. Whether the perforated lamellae may be stable in the case of ABC triblock terpolymers or not, remains unclear up to now.

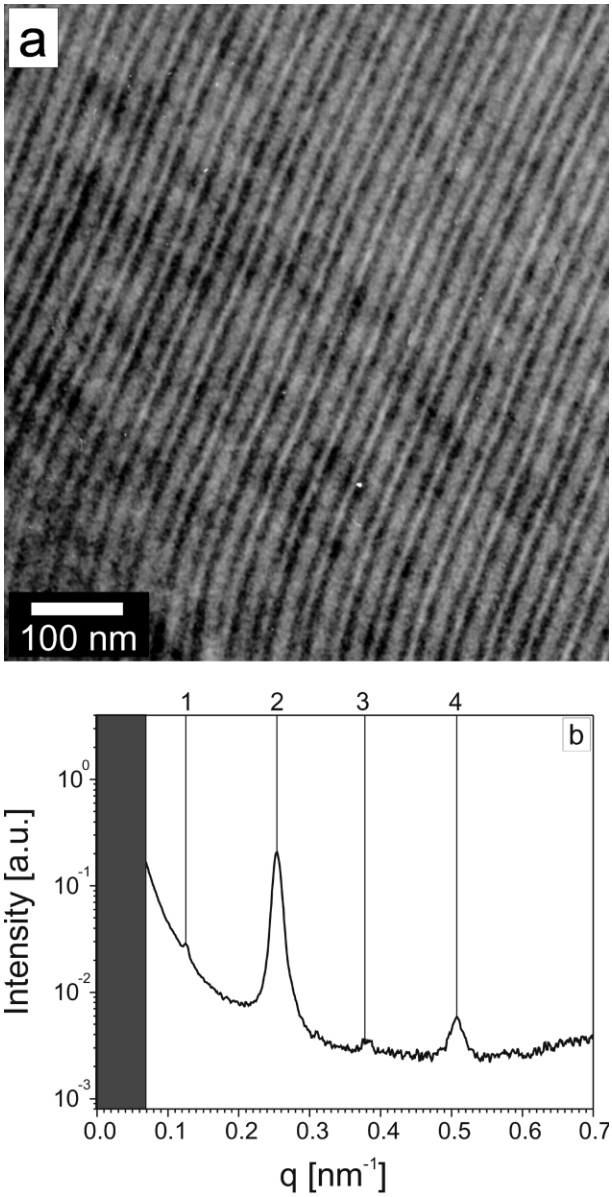

Fig. 4. $S_{30}V_{39}T_{31}^{77}$ (a) TEM micrograph, stained with I_2 (dark phase: P2VP); (b) SAXS ($q = 4\pi/\lambda \sin\theta$; λ = wavelength, 2θ = scattering angle), typical lamellar reflex positions.

3.3. $S_{30}V_{39}T_{31}^{77}$: lamellae

Further reduction of the PtBMA volume fraction leads to the formation of a lamellar microdomain structure. This can be seen in Fig. 4(a), which shows a TEM micrograph after staining with I_2. In this case, all three block components can be distinguished: P2VP appears as dark phase, the thick bright phase can be assigned to PS and the thinner phase can be assigned to PtBMA, as the latter is expected to shrink in volume due to damage in the electron beam. Shrinkage of methacrylate microdomains to less than half of the expected value have been reported [9]. The corresponding SAXS pattern of a $S_{30}V_{39}T_{31}^{77}$ sample is shown in Fig. 4(b). Higher order reflections appear at integer multiples of the first order

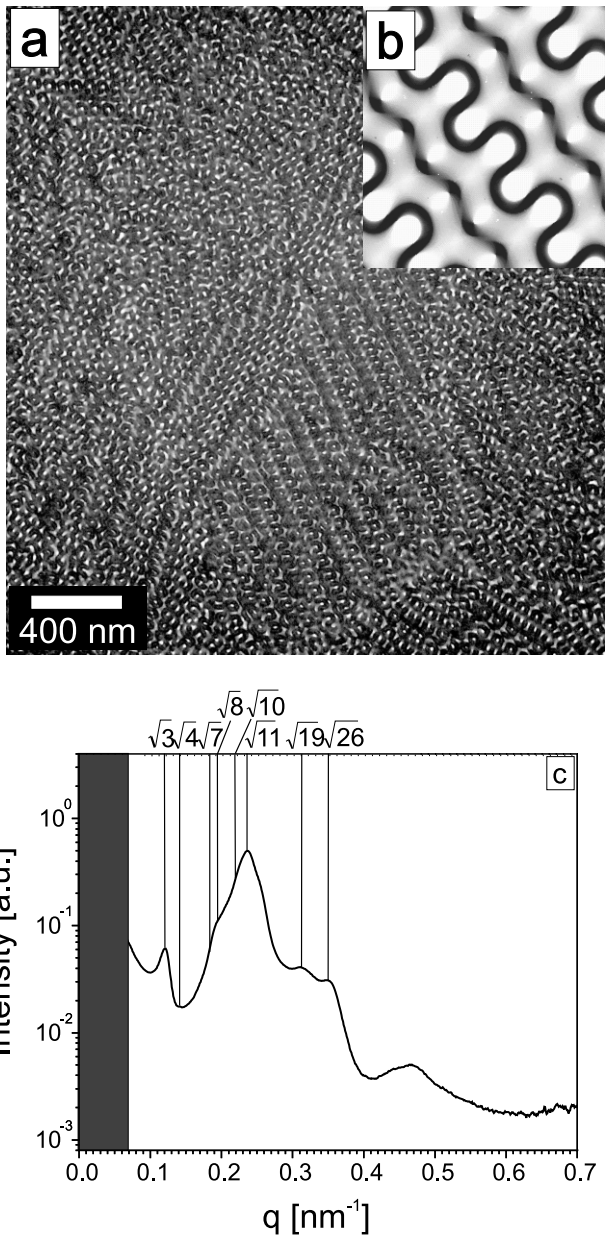

Fig. 5. $S_{32}V_{42}T_{26}^{70}$ (a) TEM micrograph, stained with I_2 (dark phase: P2VP); (b) TEMsim simulation of the [112] projection (dark matrix, translation 0, thickness 0.33) [21,22]; (c) SAXS ($q = 4\pi/\lambda \sin\theta$; λ = wavelength, 2θ = scattering angle), typical gyroid reflex positions.

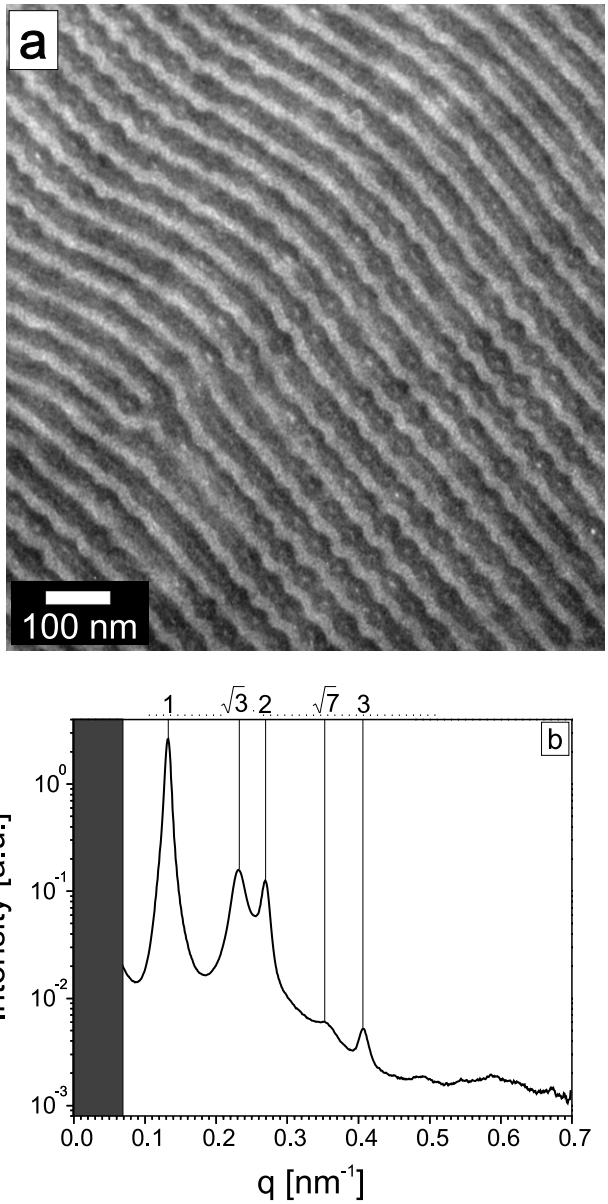

Fig. 6. $S_{37}V_{55}T_8^{78}$ (a) TEM micrograph, stained with I_2 (dark phase: P2VP); (b) SAXS ($q = 4\pi/\lambda \sin\theta$; λ = wavelength, 2θ = scattering angle), typical lamellar and cylindrical reflex positions.

peak characteristic for a lamellar structure. However, the peak intensities of the first and third order peak are rather small. This may be due to the rather small electron density contrast between the two end blocks PS and PtBMA and the same domain sizes of PS and PtBMA for this composition. If PS and PtBMA were not distinguished in the SAXS measurement, the lamellar spacing would appear to be only half of the actual triblock terpolymer periodicity and peaks would appear at positions [200], [400], …. The SAXS pattern exhibited in Fig. 4(b) can therefore be interpreted as a superposition of the actual triblock terpolymer scattering pattern and a (stronger) 'diblock copolymer' scattering pattern of only half the characteristic spacing.

3.4. $S_{32}V_{42}T_{26}^{70}$: gyroid

For $S_{32}V_{42}T_{26}^{70}$ both TEM and SAXS exhibit a gyroid morphology. The structure in Fig. 5(a) can be compared to the TEMsim simulation of the [112] projection shown in Fig. 5(b) [21,22]. The marked positions in the SAXS profile shown in Fig. 5(c) are in agreement to a cubic lattice under the assumption that the first peak corresponds to the [211] reflection. From the available data it cannot be unambiguously distinguished whether the material forms a gyroid

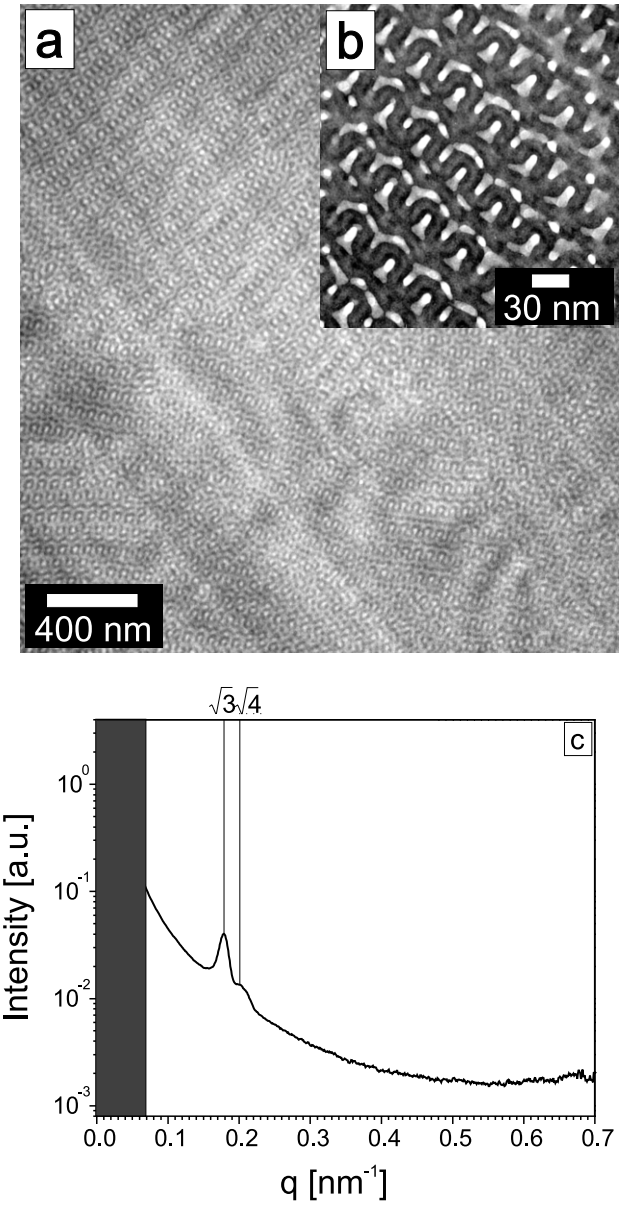

Fig. 7. $S_{38}V_{56}T_6^{76}$ (a) and (b) TEM micrographs, stained with I_2 (dark phase: P2VP); (c) SAXS ($q = 4\pi/\lambda \sin\theta$; λ = wavelength, 2θ = scattering angle), typical gyroid reflex positions.

structure consisting of interpenetrating tripod networks of the two endblocks, or if it forms yet another core-shell gyroid. However, in view of the other structures found in this series we assume the latter: an inverse core-shell-gyroid with PtBMA cores surrounded by a P2VP shell embedded within a PS matrix.

3.5. $S_{37}V_{55}T_8^{78}$: undulated lamellae

Fig. 6(a) shows a TEM micrograph of a $S_{37}V_{55}T_8^{78}$ sample after staining with I_2. The dark phase corresponds to P2VP. The structure can be described as undulated lamellae. There are small bright dots of PtBMA (minority component) within the P2VP phase, which seem to cause the undulation of the lamellae. In accordance with the SAXS pattern (Fig. 6(b)) which exhibit a hexagonal cylindrical structure ($1{:}\sqrt{3}{:}2{:}\sqrt{7}{:}3$), we assume that the PtBMA minority phase forms hexagonally arranged cylinders within the P2VP sheets of a lamellar phase. Note that the hexagonal packing of the cylinders is most likely due to the composition. A similar morphology was found before for a poly(ethylene-*alt*-propylene)-*block*-poly(ethyl ethylene)-*block*-polystyrene triblock terpolymer, where the PS cylinders were arranged on a non-hexagonal lattice [7], and in an ABC miktoarm star terpolymer [34].

Table 2
Solubility (δ) parameters at 298 K

Polymer	δ ($MPa^{1/2}$) [38,39]
Polystyrene (S)	18.5
Poly(2-vinylpyridine) (V)	20.4 [40]
Poly(*tert*-butyl methacrylate) (T)	18.0

3.6. $S_{38}V_{56}T_6^{76}$: 'diblock' gyroid

The polymer with the smallest amount of PtBMA, $S_{38}V_{56}T_6^{76}$, again shows a gyroid morphology. The structure in the micrographs in Fig. 7(a) and (b) can be related to Fig. 5(b) and the SAXS profile in Fig. 7(c) shows two maxima in the relation of $\sqrt{3}{:}\sqrt{4}$. Due to the small molecular weight of PtBMA we may assume that the two endblocks mix. Table 2 summarizes the solubility parameters (δ), which are used to estimate the corresponding segmental interaction parameters (χ) according to

$$\chi_{XY} = \frac{V}{RT}(\delta_X - \delta_Y)^2$$

with V being the segmental volume (100 cm^3/mol). The different χ-parameters are: $\chi_{SV} \approx 0.08$, $\chi_{ST} \approx 0.025$, $\chi_{VT} \approx 0.13$. Estimates of χN indicate that at these rather low molecular weights the block copolymer is located in the weak segregation limit WSL [35]. Therefore we may assume that an AB diblock or ABA triblock-like gyroid phase forms with only two interpenetrating mixed phases of PS/PtBMA separated by P2VP. Due to the relatively short blocks of PS and PtBMA the respective χN is rather low ($\chi N_{ST} \approx 7.7$ [36]). Diblock copolymers with such a degree of incompatibility would be disordered. Due to a mixing of the outer blocks there is a gain of conformational entropy of the middle block, which leads to an additional lowering of the free energy [37]. Alternatively, also miscibility between P2VP and PtBMA seems to be possible. Here $\chi N_{VT} \approx 63$ and the relative volume fraction of PtBMA is $\phi = 0.065$. Considering the asymmetric composition, a χN value about 70 should be expected for the transition from the disordered to an ordered phase (closely packed spheres), if we consider a free diblock copolymer [35]. However, the incompatible block (PS) should lower the limiting value of χN for the disordered phase of P2VP and PtBMA. Thus, a

gyroid morphology of an AB-like block copolymer, in which P2VP and PtBMA form the mixed matrix between two interpenetrating PS tripod networks seems less likely.

3.7. Diblock copolymer precursor: lamellae

In order to complete the above investigations of the systematic variation of the amount of the last block we note that TEM and SAXS data of the poly(styrene)-*b*-poly(2-vinylpyridine) precursor copolymers $S_{43}V_{57}^{52}$ and $S_{40}V_{60}^{72}$ exhibit a lamellar morphology (not shown here).

3.8. Phase diagram of SVT triblock terpolymers

We have summarized the above results in a ternary phase diagram together with sketches of the anticipated structures (Fig. 8). The colors of these sketches were chosen such as to match the grey values in the TEM images after staining with RuO_4: the black phase is PS, the grey phase is P2VP and the white phase is PtBMA. Along with the six block copolymers discussed in detail above, all other materials have been entered into the phase diagram as well.

With decreasing PtBMA volume fraction, the morphologies change from core-shell cylinders (PS core surrounded by a P2VP shell in a PtBMA matrix) via a core-shell gyroid (in coexistence to the metastable perforated lamellar phase) to a lamellar structure. In this sequence the curvature of PS/P2VP interface decreases systematically: cylinder core, gyroid core, lamellar phase. Further reduction of the PtBMA block leads yet to another gyroid structure. We believe that a tripod network of PS in a gyroid structure with two chemically different interpenetrating networks is energetically less favorable than forming the matrix in a core-shell-gyroid with PtBMA-core in a P2VP-shell ($\chi_{SV} < \chi_{VT}$). The other argument for this structure is that even with very small molecular weights of PtBMA, like in $S_{35}V_{52}T_{13}^{82}$ we receive the same characteristic results from TEM and SAXS investigations. The polymers with the smallest amounts of PtBMA exhibit the following morphologies: undulated lamellae (PtBMA cylinders within P2VP sheets of a lamellar structure) and a 'diblock gyroid' structure. In this sequence the curvature of the P2VP-PtBMA decreases. Finally the diblock precursor shows a lamellar structure which is in accordance to previous investigations [31].

We note in passing that the well-developed inverse core shell gyroid structure observed in the $S_{32}V_{42}T_{26}^{70}$ polymer may be of potential interest for the formation of a membrane with nanoscopic pore sizes. If hydrolysis of the T cores to poly(methacrylic acid) could be achieved without altering the overall morphology of the block copolymer, a 3D continuous network of a water soluble polyelectrolyte should result. The permeability through these channels may then be controlled by the pH of the respective solution.

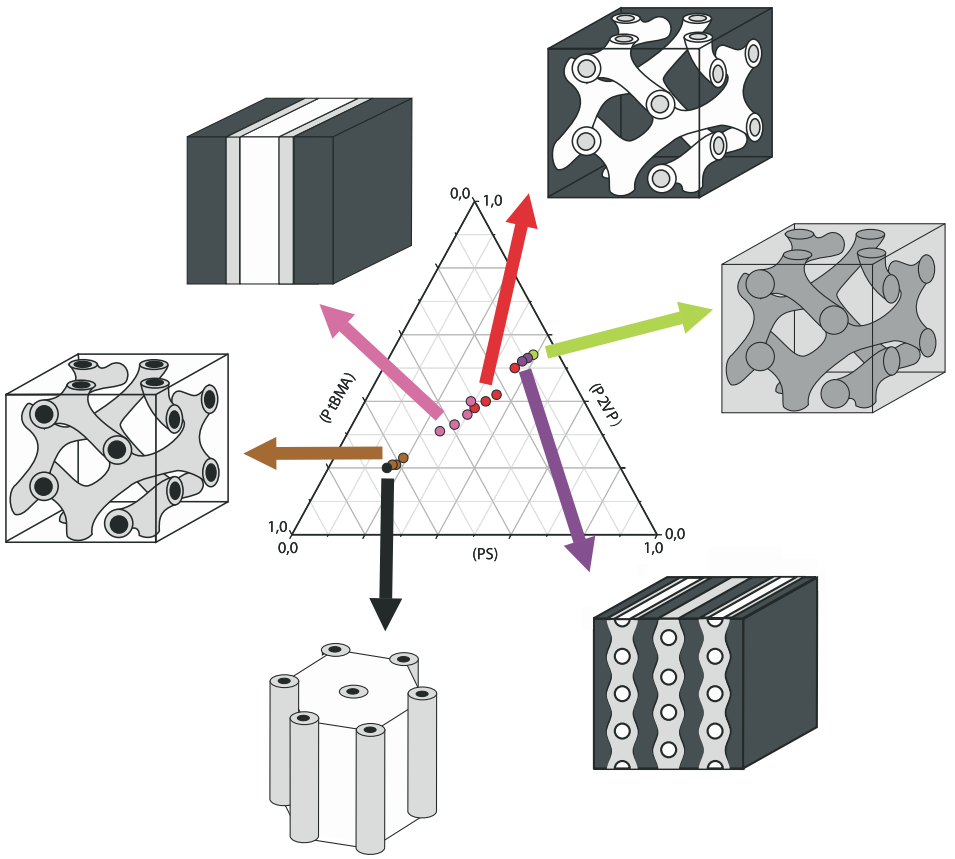

Fig. 8. Phase diagram of synthesized SVT triblock terpolymers.

This aspect, however, is beyond the scope of the present work.

4. Conclusion

The systematic variation of one block with respect to the other two blocks of an SVT triblock terpolymer reveals the following picture: starting from a symmetric composition, i.e. all three blocks have the same length, the morphology changes from lamellae via core-shell double gyroid to core-shell cylinders upon increase of the PtBMA block. These morphologies may be considered as core-shell analogues of the corresponding diblock copolymer morphologies. Upon decrease of the PtBMA block the morphological scheme is different: a slight decrease of PtBMA leads to the formation of an inverse core-shell double gyroid, but the further decrease leads to a cylinder-in-lamellae morphology, which does not have an analogue in diblock copolymers. The reason for the formation of this morphology is most likely the asymmetry of the interactions between the adjacent blocks involved. The competition of different interactions in combination with the composition is responsible for this behavior. A similar transition from a core-shell double gyroid to a cylinder-in-lamellae morphology has also been observed for poly(ethylene-alt-propylene)-*block*-poly(ethyl ethylene)-*block*-polystyrene triblock terpolymer with comparable compositions. Further decrease of the PtBMA block finally leads to a morphology comparable to binary block copolymers, where only two different microphases can be distinguished. This is due to the vanishing repulsion between the two outer blocks in combination with an entropic gain of the middle block. In future work the thin film behavior of these block copolymers will be investigated in order to set up a relationship between bulk and thin film morphologies.

Acknowledgements

The authors thank Astrid Göpfert and Carmen Kunert for their skilful help with the TEM measurements. In addition we thank Volker Urban (ESRF, Grenoble, France) for his assistance during the SAXS measurements. We thank M. Gradzielski for helpful discussions. We are grateful to the ESRF for financial support and provision of synchrotron beam time. This work was carried out in the framework of the *Sonderforschungsbereich 481* funded by the *Deutsche Forschungsgemeinschaft* (DFG).

References

[1] Stadler R, Auschra C, Beckmann J, Krappe U, Voigt-Martin I, Leibler L. Macromolecules 1995;28:3080.
[2] Bates FS, Fredrickson GH. Physics Today 1999;52:32.
[3] Abetz V. Block copolymers, ternary triblocks. In: Kroschwitz JI,, editors, 3rd ed. Encyclopedia of polymer science and technology, 1. New York: Wiley; 2003. p. 482–523.
[4] Mogi Y, Nomura M, Kotsuji H, Ohnishi K, Matsushita Y, Noda I. Macromolecules 1994;27:6755.
[5] Hückstädt H, Göpfert A, Abetz V. Polymer 2000;41:9089.
[6] Breiner U, Krappe U, Abetz V, Stadler R. Macromol Chem Phys 1997;198:1051.
[7] Neumann C, Loveday DR, Abetz V, Stadler R. Macromolecules 1998; 31:2493.
[8] Shefelbine MA, Vigild ME, Matsen MW, Hajduk D, Hillmyer MA, Cussler EL, Bates FS. J Am Chem Soc 1999;121:8457.
[9] Abetz V, Goldacker T. Macromol Rapid Commun 2000;27:6755.
[10] Elbs H, Fukunaga K, Stadler R, Sauer G, Magerle R, Krausch G. Macromolecules 1999;32:1204.
[11] Böker A, Müller AHE, Krausch G. Macromolecules 2001;34:7477.
[12] Elbs H, Drummer C, Abetz V, Hadziioannou G, Krausch G. Macromolecules 2001;34:7917.
[13] Fukunaga K, Hashimoto T, Elbs H, Krausch G. Macromolecules 2002;35:4406.
[14] Elbs H, Drummer C, Abetz V, Krausch G. Macromolecules 2002;35: 5570.
[15] Krausch G. Mater Sci Engng Rep 1995;14:1.
[16] Fasolka MJ, Mayes AM. Ann Rev Mater Res 2001;31:323.
[17] Bailey TS, Pham HD, Bates FS. Macromolecules 2001;34:6994.
[18] Giebeler E, Stadler R. Macromol Chem Phys 1997;198:3815.
[19] Sawyer LC, Grubb DT. Polymer Microscopy, 2nd ed. London: Chapman and Hall; 1996.
[20] Fit2D: http://www.esrf.fr/computing/scientific/FIT2D.
[21] TEMsim: http://www.msri.org/publications/sgp/jim/software/temsim/index.html.
[22] Hückstädt H, Goldacker T, Göpfert A, Abetz V. Macromolecules 1994;27:6755.
[23] Matsen MW. J Chem Phys 1998;108:785.
[24] Garstecki P, Holyst R. Phys Rev E 2001;64:021501.
[25] Hashimoto T. Macromolecules 1992;25:1433.
[26] Förster S, Khandpur AK, Zhao J, Bates FS, Hamley IW, Ryan AJ, Bras W. Macromolecules 1994;27:6922.
[27] Goldacker T. PhD Thesis, University of Bayreuth, 1999.
[28] Matsen MW, Bates FS. J Chem Phys 1997;106:2436.
[29] Hajduk DA, Takenouchi H, Hillmyer MA, Bates FS, Vigild ME, Almdal K. Macromolecules 1997;30:3788.
[30] Khandpur AK, Förster D, Bates FS, Hamley IW, Ryan AJ, Bras W, Almdal K, Mortensen K. Macromolecules 1996;28:8796.
[31] Schulz MF, Khandpur AK, Bates FS, Almdal K, Mortensen K, Hajduk DA, Gruner SM. Macromolecules 1996;29:2857.
[32] Hillmyer MA, Bates FS, Almdal K, Mortensen K, Ryan AJ, Faiclough JPA. Science 1996;271:976.
[33] Hillymer MA, Bates FS. Macromolecules 1996;29:6994.
[34] Hückstädt H, Göpfert A, Abetz V. Macromol Chem Phys 2000;201: 296.
[35] Matsen MW, Bates FS. Macromolecules 1996;29:1091.
[36] Schubert DW, Stamm M, Müller AHE. Polym Engng Sci 1999;39: 1501.
[37] Abetz V, Stadler R, Leibler L. Polym Bull 1996;37:135.
[38] Barton AF. CRC handbook of polymer liquid interaction parameters and solubility parameters. Boca Raton: CRC Press; 1990.
[39] Brandrup J, Immergut EH. Polymer handbook, 3rd ed. New York: Wiley; 1989.
[40] Lescanec RL, Fetters LJ, Thomas EL. Macromolecules 1998;31:1680.